Vol 18 No 3, March 2009
1674-1056/2009/18(03)/1194-07

Chinese Physics B

© 2009 Chin. Phys. Soc.
and IOP Publishing Ltd

First-principles study of the (001) surface of cubic $PbHfO_3$ and $BaHfO_3$*

Ni Guang-Xin(倪广鑫) and Wang Yuan-Xu(王渊旭)†

Institute of Computational Materials Science, School of Physics and Electronics, Henan University, Kaifeng 475004, *China*

(Received 31 June 2008; revised manuscript received 12 August 2008)

Using first-principles techniques, we investigate the (001) surfaces of cubic $PbHfO_3$ (PHO) and $BaHfO_3$ (BHO) terminated with both AO (A=Pb and Ba) and HfO_2. Surface structure, partial density of states, band structure, and surface energy are obtained. The BaO surface is found to be similar to its counterpart in BHO. For the HfO_2-terminated surface of cubic PHO, the largest relaxation appears on the second-layer atoms but not on the first-layer ones. The analysis of the structure relaxation parameters reveals that the rumpling of the (001) surface for PHO is stronger than that for BHO. The surface thermodynamic stability is explored, and it is found that both the PbO- and the BaO-terminated surfaces are more stable than the HfO_2-terminated surfaces for PHO and BHO, respectively. The surface energy calculations show that the (001) surface of PHO is more easily constructed than that of BHO.

Keywords: solid surface structure, first-principles calculation, electronic structure

PACC: 6820, 7780, 7115M, 7125

The surfaces of ABO_3 perovskite materials have been intensively investigated both experimentally[1−3] and theoretically[4−10] due to their numerous high-tech applications such as oxygen sensors, optical waveguides, substrates for high-T_c superconductors, etc. Because of their wide range of technological and industrial applications, the lead-based oxides have been extensively studied. However, only a few studies exist about the synthesis of lead hafnate PHO, despite the fact that it is structurally similar to lead zirconate ($PbZrO_3$, PZO) at room temperature and, therefore, has potential ferroelectric applications.[11−13] In addition, its mixed crystal-like $PbHf_{1-x}Ti_xO_3$ (lead hafnate titanate, PHT)[14,15] and $PbZr_{1-x}Ti_xO_3$ (lead zirconate titanate, PZT)[16] which have similar phase diagrams, exhibit intriguing properties within different phases. BHO has been well known as high melting temperature material[17] and confirmed to have a very high melting temperature (2893 K) as well as high thermal expansion coefficient (6.93×10 K) in a range between 300 to 1500 K.[18] Besides, it has a potential attraction for thermal barrier coatings (TBCs) because of its thermoelectricity and thermalconductivity properties.

As is known, surfaces may possess some special physical properties different from those of the interior of corresponding bulk due to the surface effects. Thus, it is important to investigate the surface properties of PHO and BHO by using experimental and theoretical methods. However, to our knowledge, there is no theoretical study on the (001) surface properties of cubic PHO and BHO by using the first-principles technology. In the present paper, we present electronic and atomic structures of the (001) surfaces of cubic PHO and BHO by using the density functional theory. We chose the cubic phase because it is most extensively studied in other compounds, and from the comparison between the two, we can deduce how the difference between atoms affects their surface properties. The other low symmetry phases are left to be studied as a future problem.

The calculations presented in the present work are performed within the local density approximation (LDA)[19] and the generalized gradient approximation (GGA)[20] based on the density functional theory (DFT), by using the Vienna *Ab initio* Simulation Package (VASP).[21] The projector augmented wave (PAW) method[22] with plane waves up to a cutoff energy of 500 eV is used. We use a $10\times10\times1$ mesh for the Brillouin zone integration based on the Monkhorst–Pack scheme.[23] In our calculations, two types of terminations are considered: AO (A=Pb or Ba) termination and HfO_2 termination. For the AO-terminated surface, the slab is composed of five AO layers and

*Project supported by the Natural Science Foundation of Henan University, China (Grant No 07ZRZD005) and the Foundation of Science and Technology Department of Henan Province, China (Grant No 082300410010).

†Corresponding author. E-mail: wangyx@henu.edu.cn

four HfO_2 layers and for the HfO_2-terminated one, five HfO_2 layers and four AO layers. In both cases, the slabs with nine-lattice-constant thickness are separated by a three-lattice-constant thick vacuum region. The supercells are tetragonal with space group $P4mmm$. For the AO-terminated surfaces (type-I), the first, second, third, fourth, and central layers are AO, HfO_2, AO, HfO_2, and AO, respectively while for the HfO_2-terminated one (type-II), the first, second, third, fourth, and central layers are HfO_2, AO, HfO_2, AO, and HfO_2, respectively. For both cases, the first layer refers to the surface layer. During the surface structure optimization, all atoms are fully relaxed with forces less than 0.2 eV/nm. Our calculations show that the vacuum region and the number of layers are large enough for these systems.

Before starting the surface calculation, we optimize the bulk structure by using the same method under the same computational conditions with a 10×10×10 k-point mesh. The computed lattice constants of cubic PHO and BHO with the GGA (LDA) are 0.416 (0.408) and 0.420 (0.412)nm, respectively, which match closely the experimental ones, 0.414 and 0.417 nm. We use the theoretical lattice constants in all calculations presented here.

As the surface is in equilibrium with its surroundings (HfO_2 and AO), the surface stability can be determined from the fundamental thermodynamic potential F as a function of the chemical potentials of HfO_2 and AO, μ_{HfO_2} and μ_{AO}, respectively.[24] In principle, F should be a function of the chemical potentials for A (Pb or Ba), Hf, and O_2, respectively. Since A and Hf are easily oxidizable, we just define F as a function of the chemical potentials of their oxides for each type, expressed as

$$F(\text{I or II}) = \frac{1}{2}\Big[E_{\text{slab}}(\text{I or II}) - N_{HfO_2}(\mu_{HfO_2} + E_{HfO_2}) - N_{AO}(\mu_{AO} + E_{AO})\Big], \quad (1)$$

where E_{slab}, E_{HfO_2}, and E_{AO} are the total energies of the relaxed surface structure, HfO_2 has the monoclinic structure, BaO the rocksalt structure, and PbO the hexagonal structure. N_{HfO_2} and N_{AO} are the numbers of HfO_2 and AO layers in surface structures. For the type-I surface, N_{HfO_2} and N_{AO} are 4 and 5, respectively. N_{HfO_2} and N_{AO} are 5 and 4 for the type-II one. The surfaces of $PbHfO_3$ and $BaHfO_3$ can be stable, no matter what type they are, under the conditions of

$$-E_f = \mu_{HfO_2} + \mu_{AO} \quad (2)$$

and

$$-E_f \le \mu_{HfO_2}, \quad \mu_{AO} \le 0, \quad (3)$$

where E_f is the formation energy of cubic bulk PHO or BHO and obtained from the monoclinic HfO_2 and AO (hexagonal PbO or rocksalt BaO) as

$$-E_f = E_{AHfO_3} - E_{AO} - E_{HfO_2}. \quad (4)$$

Figure 1 shows the calculated values of F for the surface structures of PHO and BHO. The calculated formation energies of cubic PHO and BHO are –0.21 and 1.22 eV, respectively. From both PHO and BHO in Fig.1 we can see that the type-I surface is more stable than the type-II one in a wide range of μ_{HfO_2}, and the type-I surface of PHO is more stable than the type-I one of BHO.

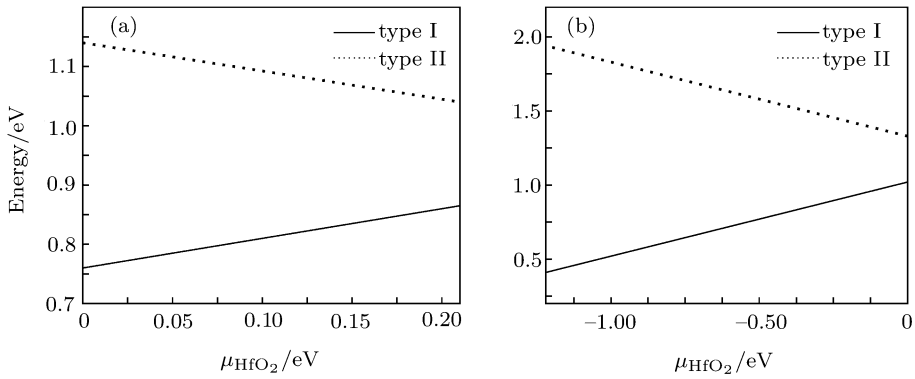


Fig.1. Curves for fundamental thermodynamic potential F as a function of the chemical potential of HfO_2, μ_{HfO_2} for the two types of surfaces of the PHO and BHO as shown in panels (a) and (b), respectively.

In the following, we will discuss the surface energy. We define $E_{\rm s}$ as the average surface energy of two types of surface terminations, i.e.

$$E_{\rm s} = \frac{1}{4}\left[E_{\rm slab(II)} + E_{\rm slab(I)} - 9E_{\rm bulk}\right], \qquad (5)$$

where $E_{\rm slab(I)}$, $E_{\rm slab(II)}$ and $E_{\rm bulk}$ are the total energies of the relaxed AO-terminated slab, the relaxed HfO_2-terminated slab, and the bulk crystal per unit cell, respectively. A factor of four comes from the fact that we create four surfaces during the cleavage procedure. The number 9 in expression (5) means that in our calculations, the two nine-layer AO- and HfO_2-terminated surfaces together represent nine bulk unit cells. The cleavage energy ($E_{\rm cle}$) and the relaxation energy ($E_{\rm rel}$) are defined respectively as

$$E_{\rm cle} = \frac{1}{4}\left[E_{\rm slab}^{\rm (unrel)}({\rm I}) + E_{\rm slab}^{\rm (unrel)}({\rm II}) - 9E_{\rm bulk}\right], \qquad (6)$$

$$E_{\rm rel}({\rm I}) = \frac{1}{2}\left[E_{\rm slab}({\rm I}) - E_{\rm slab}^{\rm (unrel)}({\rm II})\right], \qquad (7)$$

where $E_{\rm slab}^{\rm (unrel)}$ (I), $E_{\rm slab}^{\rm (unrel)}$ (II) and $E_{\rm slab}$ (I) are the total energies for the unrelaxed AO-terminated slab, the unrelaxed HfO_2-terminated slab, and the relaxed AO-terminated slab, respectively. The average surface energy, the cleavage energy, and the relaxation energy of PHO and BHO are listed in Table 1. We can see that the cleavage energies of the two materials are in a similar scale, while the relaxation energies are in different scales. The absolute value of the relaxation energy of PHO is larger than that of BHO, while the surface energy of PHO is smaller than that of BHO. The smaller surface energy means the easier cleavage under the condition where the migration of atoms can be neglected. Thus we obtain the conclusion that the surface of PHO is easier to construct than that of BHO.

Table 1. Theoretical average surface energies for PHO and BHO (in eV/a_0^2). The $E_{\rm cle}$ (in eV) denotes the cleavage energy and the $E_{\rm rel}$ (in eV) represents the relaxation energy.

	$E_{\rm cle}$ (I)	$E_{\rm rel}$ (II)	$E_{\rm s}$
PHO-GGA	1.16	–0.15	0.95
BHO-GGA	1.30	–0.07	1.17

Tables 2 and 3 summarize the calculated values of atomic relaxation parameters for terminations of the (001) surfaces of cubic PHO and BHO. The positive displacement denotes the relaxation toward the vacuum and the magnitude is measured with respect to the bulk truncated atomic positions. For the AO-terminated surfaces, the largest relaxation occurs for the surface-layer atoms, as expected. In the case of the HfO_2-termination of PHO, the largest relaxation is for the second-layer atoms but not for the first-layer ones, which is different from that of BHO. Rumpling parameter s measures the outward displacement of the first-layer oxygen with respect to the first-layer metal atoms, and Δd_{12} is the change of the first interlayer spacing, measured from the surface to the subsurface metal z-coordinate, and a similar definition is given to Δd_{23} between the second and third layers. For the HfO_2-terminated surfaces, the absolute values of s and Δd in PHO are larger than that of BHO, which means that the surface rumpling in PHO is larger than that of BHO. In the case of AO-terminations, our calculated values of s show that the rumpling for PHO is two times larger than that of BHO. This phenomenon is attributed to the fact that the large displacement of the first-layer Pb atoms results in its great surface rumpling.

Table 2. Calculated values of atomic displacement (relative to the ideal position) δ_z for the BaO (PbO)- and HfO_2-terminated surfaces of BHO (PHO). Units are in percent of the theoretical lattice constant (a_0=0.412 (0.420) and 0.408 (0.416) nm for LDA and GGA, respectively). δ_z is positive for the displacement toward the bulk.

	δ_z			δ_z		
layer	BaO (PbO)	LDA	GGA	HfO_2	LDA	GGA
1	Ba (Pb)	2.8(5.3)	2.6(4.5)	Hf	2.5(3.2)	2.8(3.2)
	O	–0.2(–0.6)	–0.0(–0.6)	O	1.3(1.3)	1.2(0.7)
2	Hf	–1.4(–2.2)	–1.5(–2.4)	Ba (Pb)	–2.4(–4.4)	–2.5(–4.8)
	O	–0.6(–0.5)	–0.7(–1.0)	O	–0.4(–0.2)	–0.2(–0.3)
3	Ba(Pb)	0.2(1.4)	0.3(1.4)	Hf	0.2(0.8)	0.5(1.0)
	O	0.2(–0.2)	0.0(–0.2)	O	–0.2(0.0)	0.1(0.2)
4	Hf	0.2(–0.4)	0.2(–0.4)	Ba (Pb)	–0.5(–0.9)	–0.3(–0.6)
	O	0.0(–0.1)	0.0(–0.1)	O	–0.1(–0.1)	0.0(0.0)

Table 3. Surface relaxation parameters (in percent of lattice constant a_0) for BHO (PHO).

	s	Δd_{12}	Δd_{23}
BaO(PbO)-termination			
BHO(PHO)-LDA	2.92(5.95)	–4.21(–7.52)	1.61(3.62)
BHO(PHO)-GGA	2.63(5.08)	–4.10(–6.81)	1.75(3.74)
HfO_2-termination			
BHO(PHO)-LDA	1.21(1.93)	–4.89(–7.59)	2.55(5.16)
BHO(PHO)-GGA	1.63(2.5)	–5.32(–7.92)	2.99(5.76)

In order to understand the reason why the displacement of the Pb atoms for PHO is larger than that of the Ba atoms in BHO during surface rumpling, we calculate the total energies of the (001) surface systems for PHO and BHO with different displacements of the Pb and Ba atoms in the surface layer, and the results are shown in Fig.2. The figure shows that the total energy of the surface structure for PHO decreases more quickly than that of BHO with the same displacement of the Pb and Ba atoms, which means that the Pb atoms in the PbO-terminated surface of PHO can move more easily or that the Pb atoms of the PHO surface with PbO-termination are more flexible.

Figure 3 illustrates the band structures of PHO. The top of the upper valence band (VB) and the bottom of the lowest conduction band (CB) for PbO-terminated surface are located at X and Γ points, respectively, and the band gap is reduced compared with that of the bulk system, 3.6 eV. The top of the upper VB for HfO_2-terminated surface is located at M point, while the bottom of the lowest CB is located at the K point, yielding an indirect gap of 2.4 eV. To further understand the behaviours of the band structures

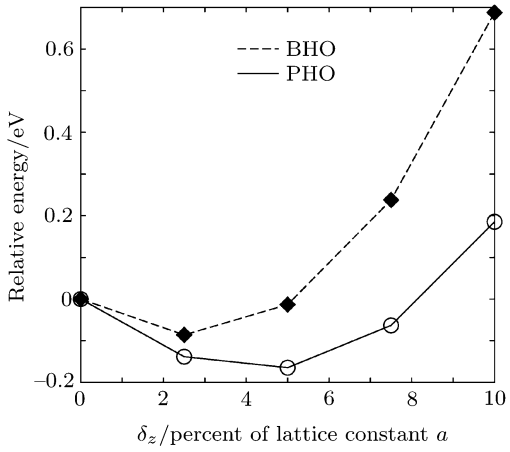


Fig.2. Curves for total energy as a function of the displacement δ_z relative to the lattice constant a_0. Pb and Ba atoms are in the first layer along the [001] direction for the AO-terminated surface structures of PHO and BHO, respectively.

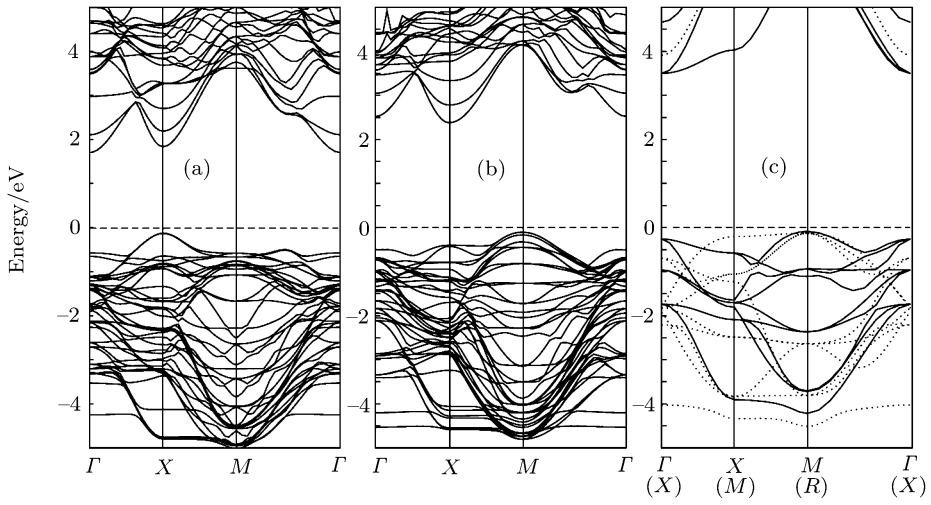


Fig.3. Curves for band structure of PH, where panels (a) and (b) represent PbO- and HfO_2-terminated surfaces of PHO, respectively; panel (c) is for the bulk system, with solid and dotted lines representing the band structure on the $\Gamma \to X \to M \to \Gamma$ and $X \to M \to R \to X$ axes, respectively, in the bulk Brillouin zone.

for the two types of surface structures, we calculate the partial densities of states of different layers for the two types, as depicted in Figs.4 and 5, respectively. The central layers can be regarded as those in the bulk, and the first-layer O atoms shift toward higher energies, which indicates that the band gap reduction of the PbO-terminated surface is mainly due to the upward movement of the first-layer O 2p states. By combining with the surface band structure, it is reasonable to consider that the surface state appears at the X point of the PbO-terminated surface. For the HfO_2-terminated surface, the third-layer O 2p states shift toward higher energies and this layer is similar to the central layer, while the first-layer O 2p states move downward with respect to the central layer. By comparing with the surface band structure, we can deduce that the surface state appears at the M point for the HfO_2-terminated surface and at the X point for the PbO-terminated one.

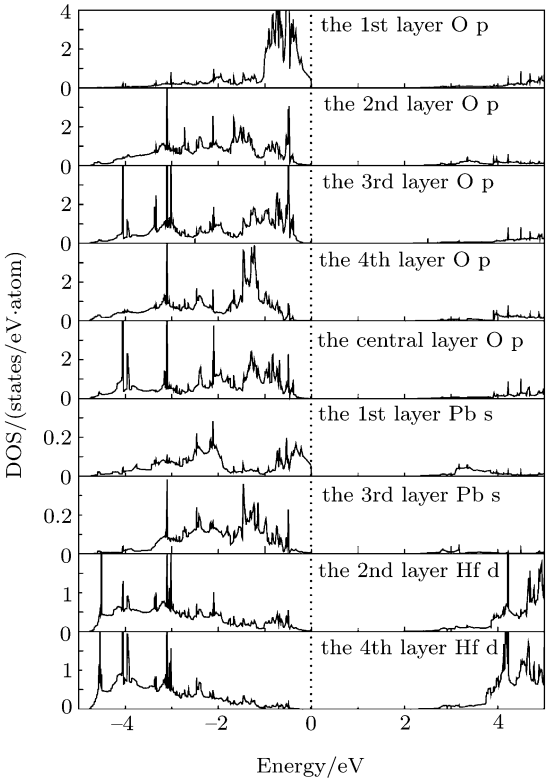


Fig.4. Partial DOSs for each layer of the PbO-terminated surface of PHO, where the dotted line represents the Fermi surface.

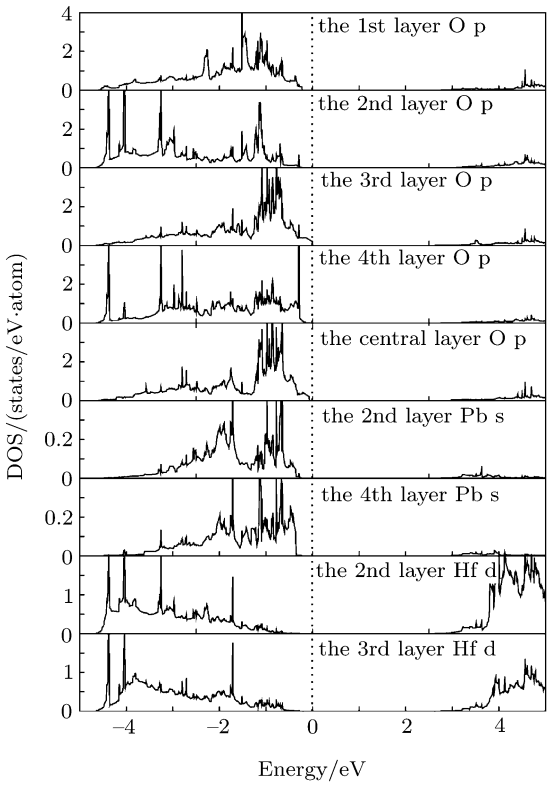


Fig.5. Partial DOSs for each layer of the HfO_2-terminated surface of PHO, where the dotted line represents the Fermi surface.

The calculated band gaps for the BaO- and HfO_2-terminated surfaces for BHO are 2.6 and 2.8 eV, respectively, which are reduced compared with the bulk value, 3.6 eV. This reduction is small compared with those for PHO as shown in Fig.6. The bulk and the BaO-terminated surface energy bands look similar to each other, and so it is difficult to distinguish the surface states from the band structures. Compared with the states in a bulk system, in the HfO_2-terminated surface, the states around the VB maximum tend to extend upward, especially at the M point. The upward shift of the valence bands in the HfO_2-terminated surface is mainly attributed to the states from the O atoms in the first layer. Thus, the surface states appearing in the HfO_2-terminated surface are caused by the O atoms in the first layer. The partial densities of states of different layers for the BaO- and HfO_2-terminated surfaces are given in Figs.7 and 8, respectively. As indicated in Fig.7, the peak of O 2p states in the surface layer has little contribution, while the central layer shifts toward high energies compared with the first layer, which indicates

that the surface state is slender and the shapes of the curves for the BaO-terminated band surface structure and the bulk system are similar to each other: the results fit the forgoing analysis well. For the HfO_2-terminated surface, compared with DOS of the O atoms in the central layer, the surface layer of O 2p states obviously shifts toward high energies, especially at the M point. It can be deduced that the surface state appears at the M point for the HfO_2-terminated surface of BHO.

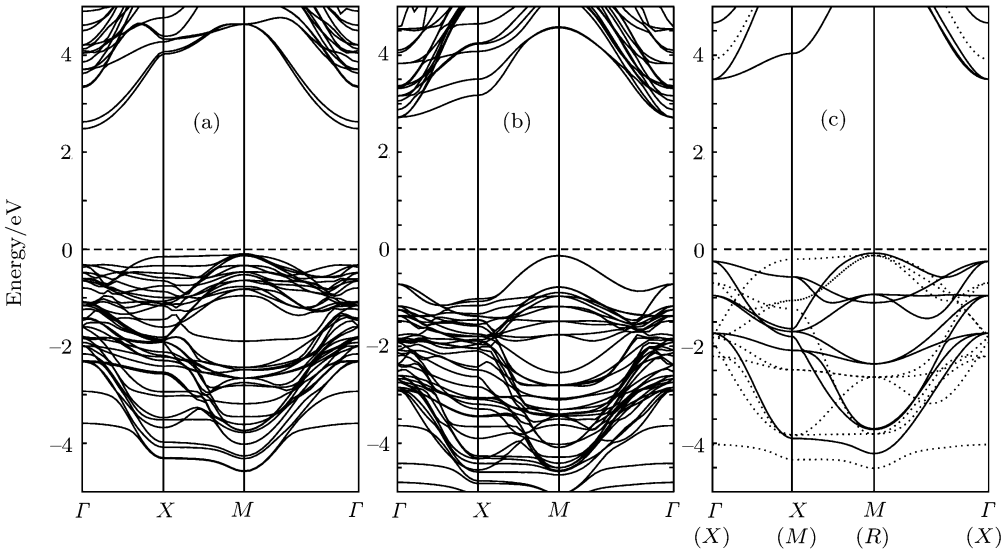


Fig.6. Curves for band structures of BHO, where panels (a) and (b) represent BaO- and HfO_2-terminated surfaces of BHO, respectively; panel (c) is for a bulk system, with the solid lines and the dotted lines representing the band structures on the $\Gamma \to X \to M \to \Gamma$ and $X \to M \to R \to X$ axes, respectively, in the bulk Brillouin zone.

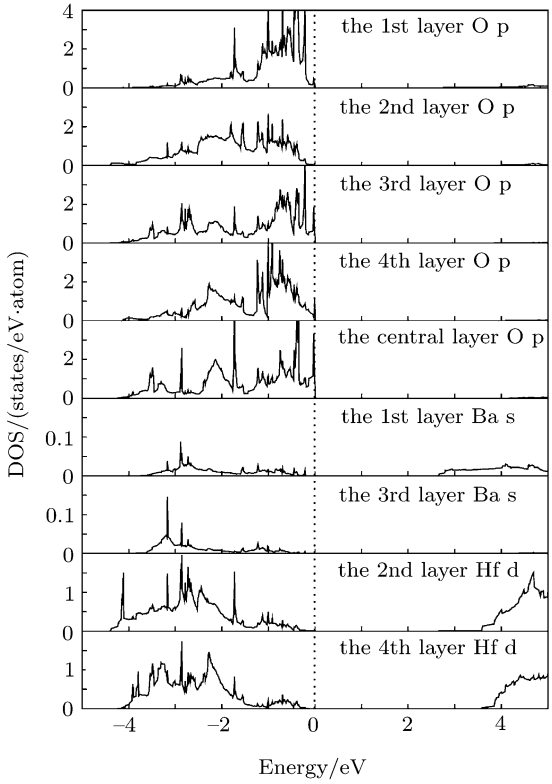


Fig.7. Partial DOSs for each layer of the BaO-terminated surface of BHO, where the dotted line represents the Fermi surface.

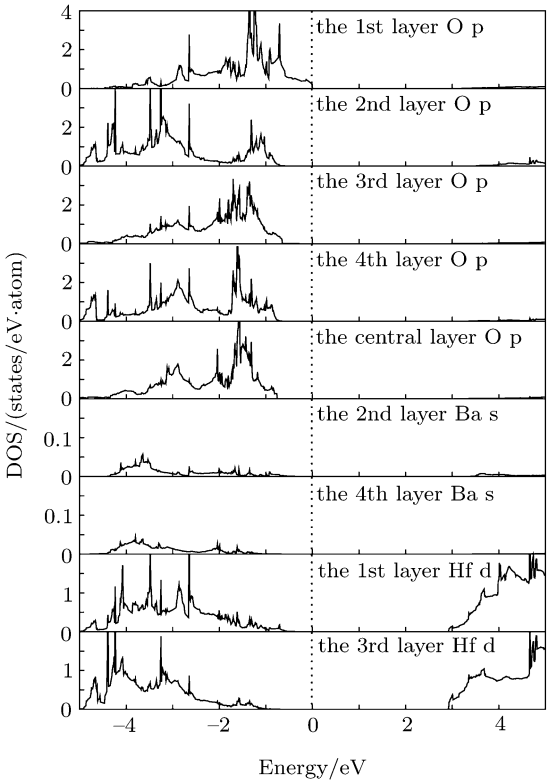


Fig.8. Partial DOSs for each layer of the HfO_2-terminated surface of BHO, where the dotted line represents the Fermi surface.

In summary, the structure and the electronic properties of the AO- and HfO_2-terminated surfaces of cubic PHO and BHO are investigated by using the projector augmented wave method within the GGA and the LDA. We find that for the HfO_2-terminated surface of PHO, the large displacement relaxation occurs in the second-layer atoms, not in the first-layer, which is different from the case of BHO. From the analysis of the structure relaxation parameters, the calculated surface rumpling of the PbO-terminated surface for PHO is much stronger than that for BHO, which is mainly due to the large displacement of the first-layer Pb atoms in PHO. The rumpling of the HfO_2-terminated surface structure for BHO is smaller than that for PHO. Comparing the band structures of the PbO-terminated and HfO_2-terminated surfaces of PHO with those of the bulk systems reveals that the surface states appear near the X and the M points of their band structures, respectively. For the HfO_2-terminated surfaces of BHO, the surface state appears at the M point. The calculated surface energies indicate that the surface of PHO is more easily constructed than that of BHO.

References

[1] Bickel N, Schmidt G, Heinz K and Müller K 1989 *Phys. Rev. Lett.* **62** 2009

[2] Hikita T, Hanada T, Kudo M and Kawai M 1993 *Surf. Sci.* **287-288** 377

[3] Maus-Friedrichs W, Frerichs M, Gunhold A, Krischok S, Kempter V and Bihlmayer G 2002 *Surf. Sci.* **515** 499

[4] Padilla J and Vanderbilt D 1997 *Phys. Rev.* B **56** 1625

[5] Cheng C, Kunc K and Lee M H 2000 *Phys. Rev.* B **62** 10409

[6] Wang Y X, Arai M and Sasaki T 2006 *Appl. Phys. Lett.* **88** 091909

[7] Wang Y X, Arai M, Sasaki T and Wang C L 2006 *Phys. Rev.* B **73** 035411

[8] Yang K, Wang C L, Li J C, Zhang C, Wu Q Z, Zhang Y F, Yin N and Liu X Y 2006 *Chin. Phys.* **15** 1580

[9] Wang Y X, Wang C L and Zhong W L 2005 *J. Phys. Chem.* B **109** 12909

[10] Heifets E, Goddard III W A, Kotomin E A, Eglitis R I and Borstel G 2004 *Phys. Rev.* B **69** 035408

[11] Corker D L, Glazer A M, Kamisky W, Whatmore R W, Dec J and Roleder K 1998 *Acta Crystallogr. Sect. B: Struct. Sci.* B **54** 18

[12] Madigou V, Baudor J L, Bouree F, Favotto C L, Roubin M and Nihoul G 1999 *Philos. Mag.* A **79** 847

[13] Roleder K, Magglione M, Fontana M D, Jamkowska-Sumara I, Kugel G E and Dec J 2000 *Ferroelectrics* **238** 139

[14] Jaffe B, Roth R S and Marzullo S 1955 *J. Res. Nat. Bur. Stds.* **55** 239

[15] Hall C A, Dungan R H and Stark A H 1964 *J. Am. Ceram. Soc.* **47** 259

[16] Jaffe B, Cook W R and Jaffe H 1971 *Piezoelectric Ceramics* (New York: Academic)

[17] Jorba M P, Tilloca G and Collongues R 1964 *Int. Symp. Magnetohydrodyn. Elec. Power Gen.* **3** 1185

[18] Maekawa T, Kurosaki K and Yamanaka S 2006 *J. Alloys Compd.* **407** 44

[19] Desclaux J P 1975 *Comput. Phys. Commun.* **9** 31

[20] Perdew J P, Burke K and Ernzerhof M 1996 *Phys. Rev. Lett.* **77** 3865

[21] Kresse G and Furthmüller J 2001 *Phys. Rev.* B **54** 11169

[22] Blöchl P E 1994 *Phys. Rev.* B **50** 17953

[23] Monkhorst H J and Pack J D 1976 *Phys. Rev.* B **13** 5188

[24] Qian G X, Martin R M and Chadi D J 1988 *Phys. Rev.* B **38** 7649